

Article

Simultaneous Electrochemical Detection of Dopamine and Ascorbic Acid Using an Iron Oxide/Reduced Graphene Oxide Modified Glassy Carbon Electrode

Teo Peik-See ¹, Alagarsamy Pandikumar ^{1,*}, Huang Nay-Ming ^{1,*}, Lim Hong-Ngee ² and Yusran Sulaiman ²

¹ Low Dimensional Materials Research Centre, Department of Physics, Faculty of Science, University of Malaya, Kuala Lumpur 50603, Malaysia; E-Mail: peps88@hotmail.com

² Department of Chemistry, Faculty of Science, Universiti Putra Malaysia, UPM Serdang, Selangor 43400, Malaysia; E-Mails: janet_limhn@yahoo.com (L.H.-N.); yusran@upm.edu.my (Y.S.)

* Authors to whom correspondence should be addressed;

E-Mails: pandikumarinbox@gmail.com (A.P.); huangnayming@um.edu.my (H.N.-M.);

Tel.: +60-1-6330-1609.

Received: 28 April 2014; in revised form: 2 July 2014 / Accepted: 11 July 2014 /

Published: 19 August 2014

Abstract: The fabrication of an electrochemical sensor based on an iron oxide/graphene modified glassy carbon electrode (Fe₃O₄/rGO/GCE) and its simultaneous detection of dopamine (DA) and ascorbic acid (AA) is described here. The Fe₃O₄/rGO nanocomposite was synthesized *via* a simple, one step *in-situ* wet chemical method and characterized by different techniques. The presence of Fe₃O₄ nanoparticles on the surface of rGO sheets was confirmed by FESEM and TEM images. The electrochemical behavior of Fe₃O₄/rGO/GCE towards electrocatalytic oxidation of DA was investigated by cyclic voltammetry (CV) and differential pulse voltammetry (DPV) analysis. The electrochemical studies revealed that the Fe₃O₄/rGO/GCE dramatically increased the current response against the DA, due to the synergistic effect emerged between Fe₃O₄ and rGO. This implies that Fe₃O₄/rGO/GCE could exhibit excellent electrocatalytic activity and remarkable electron transfer kinetics towards the oxidation of DA. Moreover, the modified sensor electrode portrayed sensitivity and selectivity for simultaneous determination of AA and DA. The observed DPVs response linearly depends on AA and DA concentration in the range of 1–9 mM and 0.5–100 μM, with correlation coefficients of 0.995 and 0.996, respectively. The detection limit of (S/N = 3) was found to be 0.42 and 0.12 μM for AA and DA, respectively.

Keywords: graphene; magnetite; dopamine; ascorbic acid; biosensor; electrochemical sensor

1. Introduction

Dopamine (DA) is one of the most important catecholamine neurotransmitters which are produced in the adrenal glands and several area of the brain. Moreover, DA is found to be the most abundant catecholamine that belongs to the family of inhibitory neurotransmitters involved in the central nervous, renal, hormonal and cardiovascular systems. Low levels or abnormalities in the DA concentration may lead to several neurological diseases, such as schizophrenia, Parkinson's disease [1], attention deficit hyperactivity disorder (ADHD) [2], restless legs syndrome (RLS) [3] and drug addiction. Owing to the strong electrochemical activity of DA, the determination of DA at sub-micro molar concentration level has gained immense attention among numerous researchers. Several methods have been developed for DA detection, including high performance liquid chromatography [4], chemiluminescence [5] and gas chromatography-mass spectrometry [6]. However, these analytical techniques have some limitations, such as being time-consuming, low-sensitivity and requiring expensive equipment, although they represent effective strategies for the detection of DA. Electrochemical sensors are a preferred alternative method because of their simple operation, fast response, time savings, low-cost, high-sensitivity, excellent selectivity and real-time detection. However, the electrochemical determination of DA is hindered by the coexistence of interfering compounds, such as ascorbic acid (AA) and uric acid (UA) in neural biological environment. Ascorbic acid, another electroactive species that plays an important role as an antioxidant in human metabolism, is the main interfering species that coexists with DA in the central nervous system. Through the electrochemical method, it is difficult to selectively sense the DA in the presence of high concentration levels of AA, because these two species are sharing nearly the same oxidation potential on the bare electrode, which results rather poor selectivity and sensitivity of DA detection [7].

In the traditional electrochemical sensor method, direct determination of DA is rare and causes poor DA response. Thus, the chemical modification of electrode surfaces has been developed to enhance the sensitivity and selectivity of electrochemical sensors. In recent years, sensing materials with high stability, good catalytic and excellent conductivity, such as polymers [8], carbonaceous materials [9] and metal oxide nanoparticle-based [10] nanocomposites have been successfully reported for the modification of bare GC electrode surfaces. Recently, carbonaceous material-modified electrode based electrochemical sensors have received widespread attention. Among them, graphene is extensively used to detect a wide range of analytes. Graphene is a two-dimensional (2D) one atom thick single layer of sp^2 -bonded carbon atoms densely packed in a honeycomb lattice [11] and it possesses high specific surface area, excellent thermal conductivity, extraordinary electrocatalytic activity and high charge mobility. Hence, the graphene-based nanocomposites hold great promise as ideal candidate sensing platforms for the development of electrochemical sensors and biosensors [12]. Magnetite (Fe_3O_4) nanoparticles with amazing properties *viz.* biocompatible, strong super-paramagnetic nature, low-toxicity and easy separation have gained much attention as catalysts in the fields of biomedical, biotechnological and sensing [13–18]. However, pure magnetite nanoparticles are chemically unstable

and easily oxidize and hence they hinder their special properties in applications. Thus, incorporation of magnetite onto the graphene sheets will give rise to new and enhanced functionalities that show favorable magnetic properties, increased electrocatalytic activity and electron transfer ability as well as prevent the heavy aggregation [19].

Based on the above facts, we report herein a simple, cost-effective and green approach for the preparation of magnetite graphene ($\text{Fe}_3\text{O}_4/\text{rGO}$) nanocomposites by using *in-situ* one-step chemical method at room temperature. The as-prepared $\text{Fe}_3\text{O}_4/\text{rGO}$ nanocomposites are used to construct modified electrodes for the simultaneous detection of DA and AA. The fabricated electrochemical sensor has exhibited rapid response, selectivity and sensitivity towards the determination of DA in the presence of AA.

2. Experimental Section

2.1. Chemicals and Reagents

Graphite flakes were purchased from Ashbury Inc. (Charlottesville, VA, USA), Sulphuric acid (H_2SO_4 , 98%), potassium permanganate (KMnO_4 , 99.9%), hydrogen peroxide (H_2O_2 , 30%), iron (II) sulphate ($\text{FeSO}_4 \cdot 7\text{H}_2\text{O}$, 99.5%) and ammonium hydroxide (NH_4OH , 25%) were purchased from System (Shah Alam, Selangor). 3-Hydroxytyraminium chloride (dopamine, DA) and L-(+)-ascorbic acid (AA) were purchased from Merck (New York, NY, USA). Potassium hexacyanoferrate (III) ($\text{K}_3[\text{Fe}(\text{CN})_6]$) was purchased from Sigma Aldrich (St. Louis, MO, USA). All other chemicals were of analytical grade and used without further purification. Stock solutions of DA and AA were freshly prepared using doubly-distilled (DI) water and used for electrochemical studies.

2.2. Characterization Techniques

Surface morphology of $\text{Fe}_3\text{O}_4/\text{rGO}$ nanocomposites was examined through a FEI Nova NanoSEM 400 FESEM (Hillsboro, CA, USA) and Hitachi H-7100 (Tokyo, Japan) transmission electron microscope (TEM). Electrochemical studies such as cyclic voltammetry (CV), differential pulse voltammetry (DPV) and electrochemical impedance spectroscopy (EIS) were performed in VersaSTAT 3 electrochemical analyzer (Princeton Applied Research, Oak Ridge, TN, USA) with a conventional three-electrode system. Glassy carbon (GCE, 3 mm in diameter), Ag/AgCl and Pt wire were used as working, reference and counter electrode, respectively. Phosphate buffer solution (0.1 M) was used as a supporting electrolyte. All the electrochemical measurements were carried out at room temperature under nitrogen atmosphere.

2.3. Preparation of Magnetic rGO ($\text{Fe}_3\text{O}_4/\text{rGO}$) Nanocomposites

Initially, graphene oxide (GO) was synthesized from graphite using a simplified Hummers' method [20]. A GO (25 mg) was dispersed in DI water under sonication for 20 min. Then, 25% NH_4OH solution was added dropwise into the GO solution to attain a pH value between 11 and 12. Later, the FeSO_4 solution was slowly introduced into the GO solution under vigorous stirring at room temperature and the stirring was continued overnight. Finally, the black-coloured solution was centrifuged, washed three times with DI water for 10 min at 4000 rpm to remove the excess

ammonium ions and then dried in a vacuum oven. The Fe_3O_4 NPs was obtained *via* the same procedure in the absence of GO and labelled as F20. Similarly, rGO was prepared through the same process without adding FeSO_4 and labelled as G1. In the present study, $\text{Fe}_3\text{O}_4/\text{rGO}$ nanocomposite was prepared by varying the weight ratios between the GO and FeSO_4 and was denoted as G1FX, where X is the weight ratio of FeSO_4 to GO. For the sake of convenience, four kinds of $\text{Fe}_3\text{O}_4/\text{rGO}$ was prepared by fixing GO as constant with varying FeSO_4 content ($m\text{GO}: m\text{FeSO}_4 = 1:2, 1:5, 1:10, 1:20$) and they were labelled as G1F2, G1F5, G1F10 and G1F20, respectively.

2.4. Fabrication of $\text{Fe}_3\text{O}_4/\text{rGO}$ Modified GCE

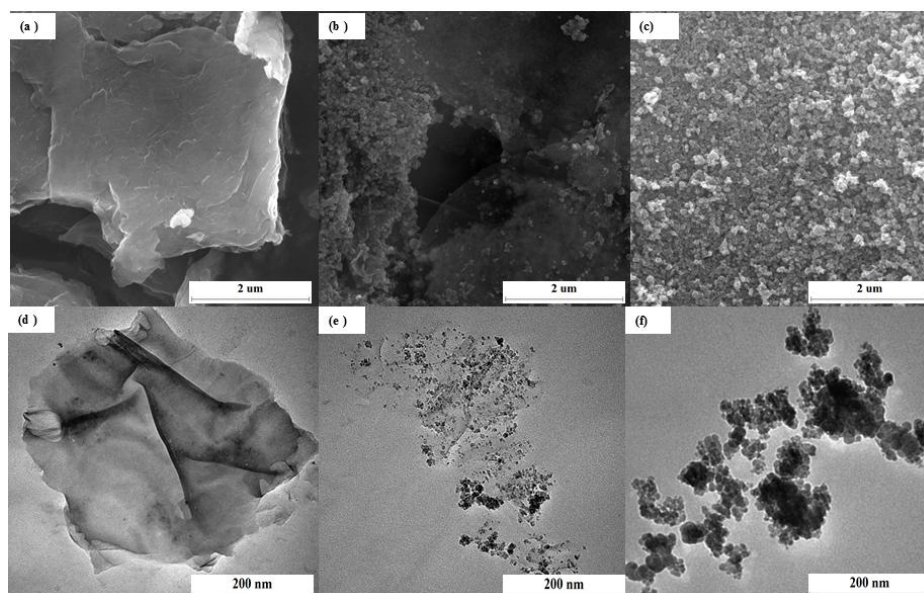
Prior to the modification, the surface of the bare GCE was polished by alumina suspension (0.05 μm) on a micro cloth polishing pad which was thoroughly rinsed with water and ultrasonically cleaned using DI water. $\text{Fe}_3\text{O}_4/\text{rGO}$ (1.5 mg) was added into DI water (1 mL) and then sonicated for 1 h to get a homogeneous suspension. An aliquot (5 μL) of the suspension was drop casted on the GCE surface and dried in oven at 60 $^\circ\text{C}$.

3. Results and Discussion

3.1. Characterization of $\text{Fe}_3\text{O}_4/\text{rGO}$ nanocomposites

The synthesis pathway of $\text{Fe}_3\text{O}_4/\text{rGO}$ nanocomposites involved the redox reaction between the GO and Fe^{2+} ions from FeSO_4 solution. During the synthesis process, the strong oxidizing agent, GO increased the oxidation state of Fe^{2+} ions to Fe^{3+} , and eventually formed into $\text{Fe}_3\text{O}_4/\text{rGO}$ nanocomposites through spontaneously *in-situ* deposition of Fe_3O_4 nanoparticles onto the reduced graphene oxide (rGO) sheets. To investigate morphological features of the prepared G1, F20 and $\text{Fe}_3\text{O}_4/\text{rGO}$ nanocomposites, FESEM and TEM images were recorded and are shown in Figure 1.

Figure 1. FESEM images of (a) G1, (b) $\text{Fe}_3\text{O}_4/\text{rGO}$ and (c) F20; TEM images of (d) G1, (e) $\text{Fe}_3\text{O}_4/\text{rGO}$ and (f) F20.

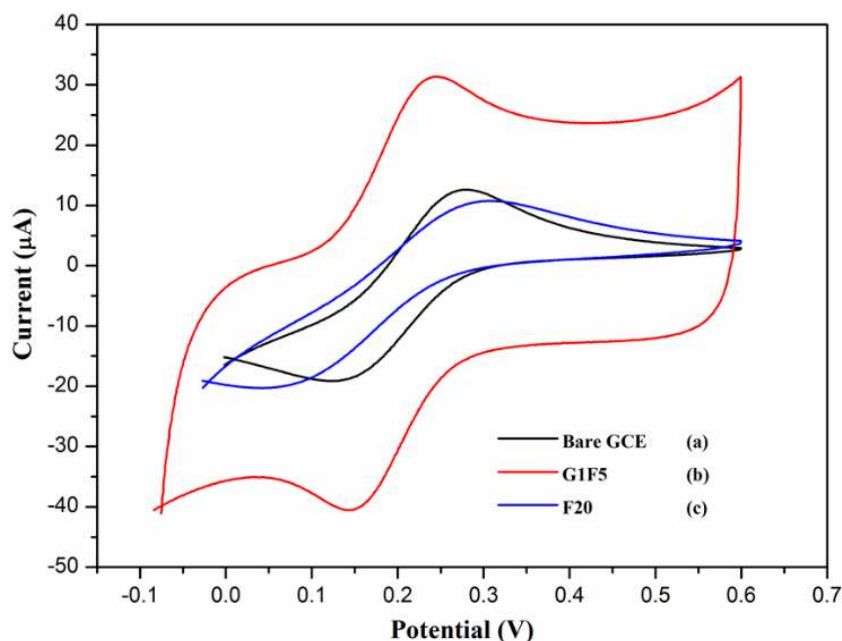


The G1 depicts a smooth surface with a wrinkled paper-like appearance (Figure 1a,d). Dispersion of Fe_3O_4 nanoparticles on the surface of rGO sheets has indicated a strong interaction obtained between rGO sheets and nanoparticles (Figure 1b,e). Whereas, the F20 are agglomerated that leads to larger size particles (Figure 1c,f) [21].

3.2. Electrochemical Behavior of $\text{Fe}_3\text{O}_4/\text{rGO}$ Electrode

The electrochemical behavior of different modified electrodes was investigated to elucidate their electron transfer behavior in the presence of $\text{K}_3[\text{Fe}(\text{CN})_6]$ as a redox probe. The cyclic voltammograms for different electrodes, which are shown in Figure 2, were recorded in the presence of 5 mM $\text{K}_3[\text{Fe}(\text{CN})_6]$ and 0.1 M KCl at a scan rate of 100 mV/s. A pair of well-defined redox peak is observed with a peak to peak separation (ΔE_p) of 140 mV for bare GCE, whereas the ΔE_p exhibited by the G1F5/GCE and F20/GCE is about 89 and 230 mV, respectively. When compared to the bare GCE, the redox peak current has increased significantly for the $\text{Fe}_3\text{O}_4/\text{rGO}/\text{GCEs}$. This improved electrochemical behavior can be attributed to the excellent electrical conductivity of the $\text{Fe}_3\text{O}_4/\text{rGO}$ present on the electrode surface. The graphene with superior electrical conductivity and unique electron transport property could accelerate the electron transfer rate at the electrode/electrolyte interface. Only at F20/GCE, was a lower redox peak current observed than that of the bare GCE, owing to the rapid aggregation of nanoparticles that leads to larger particles (Figure 1c), which may significantly diminish the electrochemical properties of the electrode and hence be electroinactive [22–24].

Figure 2. Cyclic voltammogram obtained for (a) bare GCE; (b) G1F5 and (c) F20 in the presence of 5 mM $\text{K}_3[\text{Fe}(\text{CN})_6]$ and 0.1 M KCl solution at a scan rate of 100 mV/s.



Electrochemical impedance spectroscopy (EIS) is an effective tool to probe the interfacial properties of surface-modified electrodes. Figure 3 shows the Nyquist plots observed for different electrodes in the presence of 5 mM $[\text{Fe}(\text{CN})_6]^{3-/4-}$ solution containing 0.1 M KCl in the frequency range from 10^{-1} to 10^4 Hz. A Randels equivalent circuit was used in the EIS spectra to obtain value of

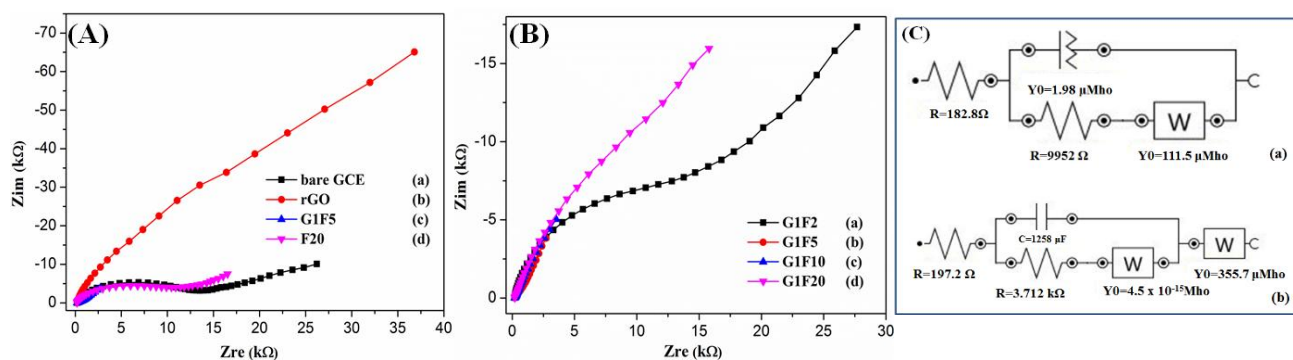
charge transfer resistance (R_{ct}), where the R_s , R_{ct} , W and Q_{CPE} refer to the solution resistance, charge transfer resistance, Warburg impedance and constant phase element, respectively (Figure 3C) and their corresponding parameters are summarized in Table 1 [25]. The F20/GCE (Figure 3A(d)) showed a large and remarkable increase in the semicircle diameter. The high resistance (9.95 k Ω) that might cause by the aggregated Fe_3O_4 could diminish the electron transfer process. The rGO/GCE showed a straight line and suggests that graphene sheets can facilitate the electron transfer process. However, coupling the magnetic particles with graphene sheets, the EIS of modified electrodes display almost a straight line, indicating low interfacial electron transfer resistance and promotion of electron transfer process for the nanocomposites (Figure 3B). This may be attributed to the larger surface area and good conductivity of the Fe_3O_4 /rGO nanocomposites [26,27]. Among the different composition of Fe_3O_4 /rGO, the G1F5 showed very small straight line due to the high interfacial electron transfer process and low charge transfer resistant.

Table 1. EIS fitting parameters for modified electrodes.

Electrochemical Impedance Fitting Parameters				
Electrodes	R_s (Ω)	Q_{CPE} (F)	R_{ct} (Ω)	W
G1F5	197.2	1.26×10^{-3}	3.7×10^{-3}	3.56×10^{-4}
F20	182.8	1.98×10^{-6}	9952	1.11×10^{-4}

Footnotes: R_s —Solution resistance; Q_{CPE} —constant phase element; R_{ct} —Charge transfer resistance; W —Warburg impedance.

Figure 3. (A) Nyquist plots obtained for (a) bare GCE, (b) rGO, (c) G1F5 and (d) F20; (B) Nyquist plots for Fe_3O_4 /rGOs (a) G1F2, (b) G1F5, (c) G1F10 and (d) G1F20 in the presence of 5 mM $K_3[Fe(CN)_6]/K_4[Fe(CN)_6]$ (1:1) solution containing 0.1 M KCl; (C) Equivalent electrical circuit for (a) F20 and (b) G1F5.



3.3. Electrocatalytic Response of Fe_3O_4 /rGOnanocomposite Modified Electrodes towards the Oxidation of Dopamine (DA)

The electrochemical behavior of different modified electrodes in the presence of 0.1 mM DA in 0.1 M PBS (pH 6.5) was investigated by cyclic voltammetric (CV) technique at a scan rate of 100 mV/s. Figure 4A shows the CV responses obtained for the bare GCE, Fe_3O_4 /rGO/GCE and F20/GCE in the presence of 0.1 mM DA. At a bare GCE, a well-defined redox peak was observed with the anodic and cathodic peaks at 257 mV and 148 mV, respectively. For the Fe_3O_4 /rGO/GCEs, the oxidation peak

currents were increased remarkably and the oxidation peak potentials were shifted negatively. Among the modified electrodes, the G1F5/GCE displays an enhanced electrochemical performance towards the oxidation of DA. The oxidation peak potential was negatively shifted to 234 mV with a dramatically enhanced oxidation peak current of 60.98 μA in comparison to the F20/GCE (2.87 μA) and bare GCE (2.79 μA). For comparison, electrocatalytic oxidation of DA also carried out with the $\text{Fe}_3\text{O}_4/\text{rGO}/\text{GCEs}$ (Figure 4B), among them the G1F5/GCE showed higher current response than that of the other composition and these results indicate that the G1F5/GCE has high electrocatalytic activity towards the oxidation of DA. It is believed that the existence of graphene is an ideal support material and acts as an effective electron promoter for electrocatalytic oxidation of DA. Good synergistic effects emerged between Fe_3O_4 nanoparticles and graphene sheets enhance the conductive area and electron transfer rate between DA and electrode surface. The redox electrochemistry of DA and its oxidized form, dopaminequinone (DAQ) was studied and the proposed mechanism [28] for electrochemical behavior of dopamine is shown in Figure 5. DA is easily oxidized electrochemically and forms DAQ. When a potential is applied to the electrode, DA is easily oxidized to form DAQ after exchange of 2 electrons and 2 protons. These electrons are later donated to the electrode and produce faradaic current [29,30].

Figure 4. (A) CVs observed for (a) bare GCE, (b) G1F5 and (f) F20; (B) CVs for (a) G1F2, (b) G1F5, (c) G1F10 and (d) G1F20 in the presence of 0.1 M PBS (pH 6.5) containing 0.1 mM DA at a scan rate of 100 mV/s.

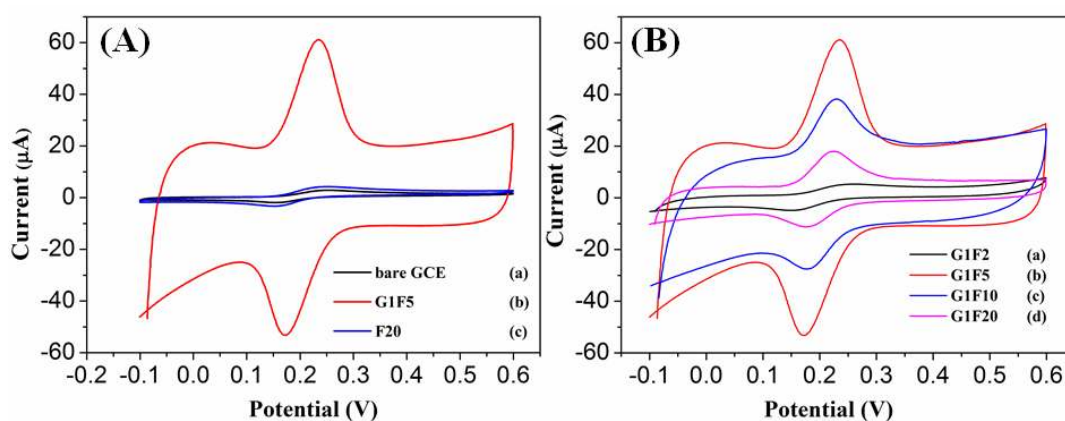
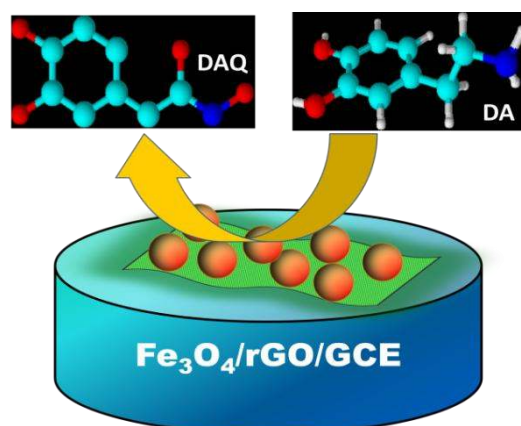


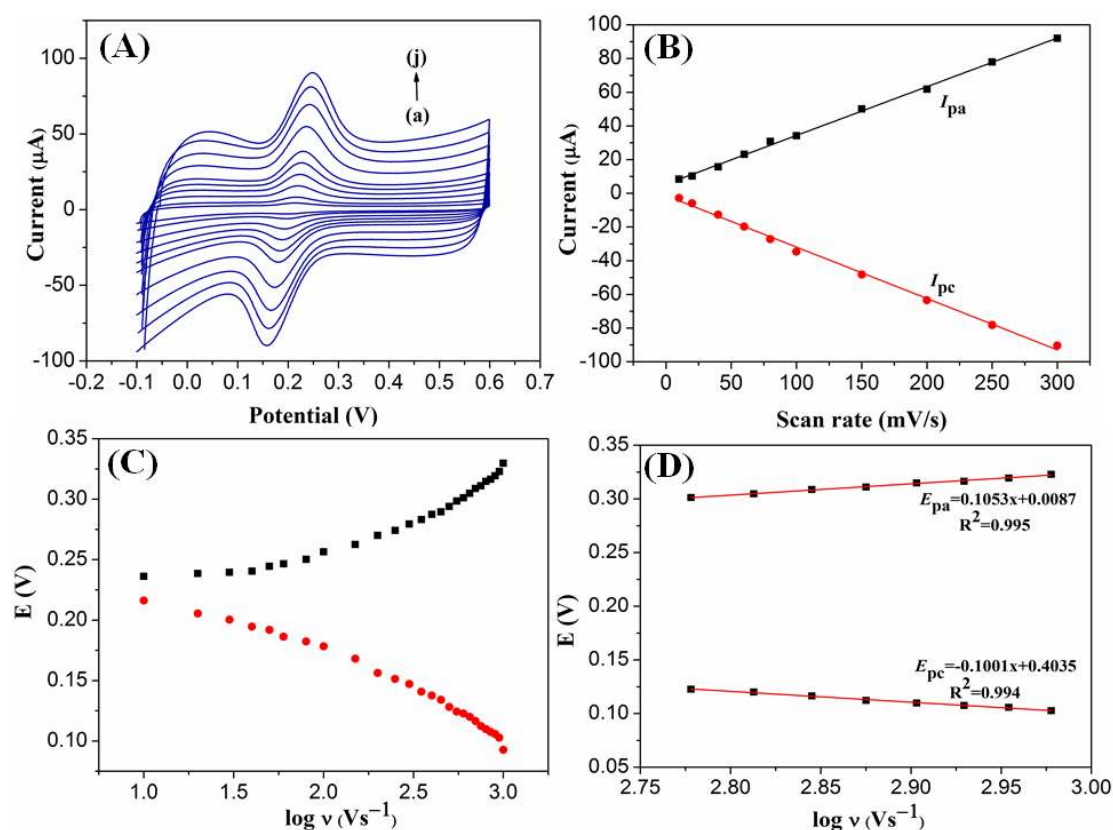
Figure 5. Electrocatalytic oxidation of dopamine at $\text{Fe}_3\text{O}_4/\text{rGO}/\text{GCE}$ electrode.



3.4. Effect of Scan Rate on the Electrocatalytic Oxidation of DA at G1F5/GCE Electrode

The influence of scan rates on the electrocatalytic response of G1F5/GCE electrode towards DA oxidation was examined and the results are shown in Figure 6A. It can be clearly observed that the oxidation peak currents are increased linearly while the oxidation peak potential was shifted positively with scan rate in the range from 10–300 mV/s (Figure 6A).

Figure 6. (A) CVs observed for G1F5/GCE in 0.1 M PBS (pH 6.5) containing 0.1 mM DA at various scan rates ((a)–(j): 10, 20, 40, 60, 80, 100, 150, 200, 250 and 300 mV/s); (B) The plots of peak current *versus* the scan rates; (C) Variation of E_p *versus* the logarithm of scan rate; (D) Variation of E_p *versus* the logarithm of the high scan rates: 600, 650, 700, 750, 800, 850, 900 and 950 mV/s.



From the CVs at modified electrode, both the values of redox peak currents (I_{pa} and I_{pc}) are linearly proportional to the increasing scan rates, with linear equations of I_{pa} (μA) = $0.2917 + 5.144v$ (mV/s) ($n = 10$, $R = 0.9997$) and I_{pc} (μA) = $0.3022 - 2.061v$ (mV/s) ($n = 10$, $R = 0.9997$), respectively for the DA oxidation (Figure 6B). These results reveal that the electrochemical oxidation of DA at modified electrode is a typical surface adsorption-controlled process. Furthermore, a linear correlation was obtained between peak potentials (E_p) and logarithm of the scan rates. For an adsorption-controlled process, the charge transfer coefficient (α) and the apparent heterogeneous electron transfer rate constant (k_s) can be calculated from the variation of E_{pa} and E_{pc} with the logarithm of the scan rate (Figure 6C) follows the Laviron's model. Two linear regression equations of E_{pa} and E_{pc} on $\log v$ are plotted (Figure 6D) and expressed as E_{pa} (v) = $0.1053 \log v + 0.0087$ ($\gamma = 0.995$) and

E_{pc} (v) = $-0.1001 \log v + 0.4035$ ($\gamma = 0.994$), respectively. The E_p values are proportional to the logarithm of the scan rates, which is higher than 600 mV/s. The slope of the linear equation is equal to $-2.3RT/\alpha nF$ and $2.3RT/(1-\alpha)nF$ corresponding to the cathodic and anodic peak, respectively which can be used to evaluate the kinetic parameters, α_c and α_a . R, T and F are referred to gas, temperature and Faraday constant, respectively. Here, the anodic transfer coefficient (α_a) is found out to be 0.44. Meanwhile, the electron transfer rate constant (k_s) is calculated to be 2.09 s^{-1} using the following Laviron's equation [31]:

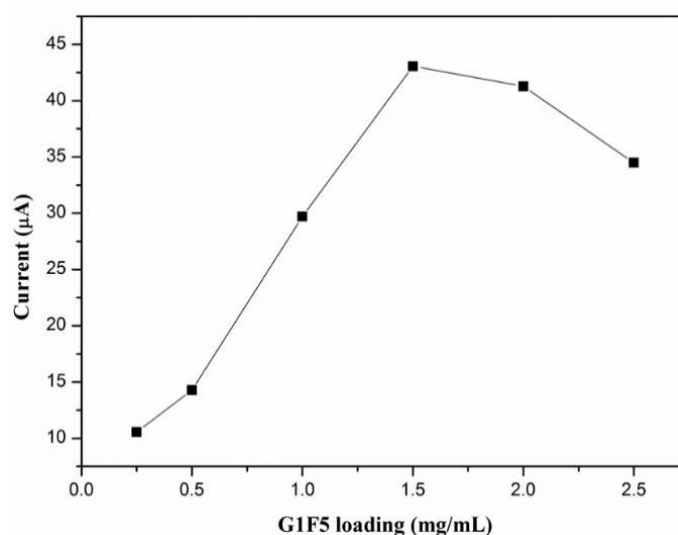
$$\log k_s = \alpha \log (1 - \alpha) + (1 - \alpha) \log \alpha - \log \frac{RT}{nFv} - \frac{\alpha(1 - \alpha)nF\Delta E_p}{2.3RT}$$

The calculated k_s value was higher than some reported values [32–34], indicating the G1F5/GCE modified electrode exhibited fast electron transfer rate towards the electrochemical oxidation of DA.

3.5. Effect of G1F5 Concentration on the Electrocatalytic Activity

The influence of G1F5 loading on the electrode surface towards the oxidation of DA was studied and the observed results are displayed in Figure 7. During the electrochemical measurement, the G1F5 volume was initially fixed as 5 μL . It is clearly seen from Figure 7 that the oxidation current response increased significantly when the concentration of G1F5 suspension increased from 0.25 mg/mL to 2.5 mg/mL due to the enhancement of the conductive surface area that influences the electron transfer rate. However, further increase of the concentration of G1F5 suspension above 1.5 mg/mL leads to a decrease in the oxidation peak current response of DA. This could be ascribed to the mass transport limitation of DA inside a thicker film and an increased mass of graphene on the electrode surface beyond the optimum level results in a shift in the oxidative over-potential towards electropositive regions and also decreases the current response [35,36]. Hence, the concentration of 1.5 mg/mL G1F5 was chosen to modify the electrode.

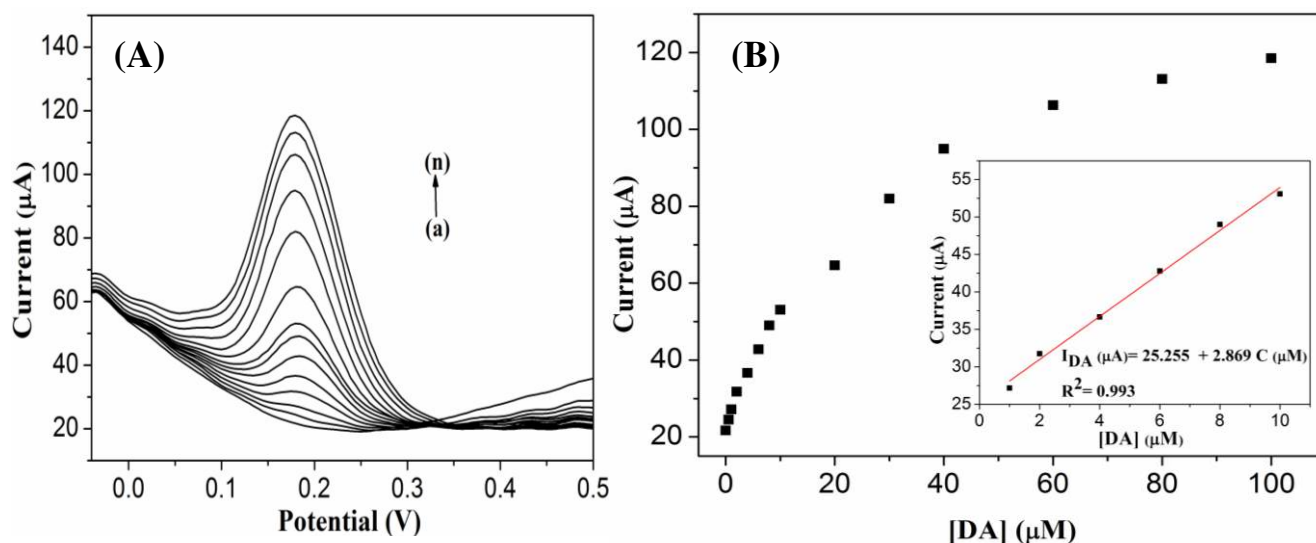
Figure 7. Effect of G1F5 amount on the current response of 0.1 mM DA in 0.1 M PBS (pH 6.5) at a scan rate of 100 mV/s.



3.6. Electrochemical Detection of DA at the G1F5 Modified Electrodes

The G1F5-modified GC electrode was utilized for the electrochemical detection of DA using the differential pulse voltammetry (DPV) technique. Figure 8A depicts the anodic peak current responses observed for oxidation of various concentrations of DA in the presence of G1F5/GCE. Significantly, the anodic peak current response was increases linearly with the addition of DA in the range of 0.5–100 μM (Figure 8B). The linear regression equation was expressed as $I_{\text{DA}} (\mu\text{A}) = 25.255 + 2.869 C (\mu\text{M})$ with a correlation coefficient of 0.993 ($n = 14$), and the detection limit ($S/N = 3$) was estimated to be 0.7 μM .

Figure 8. (A) DPV response of G1F5/GCE modified electrode with increasing the concentration of DA (from a to n: 0, 0.5, 1, 2, 4, 6, 8, 10, 20, 30, 40, 60, 80 and 100 μM). (B) The relationship between the oxidation peaks current against DA concentrations (0.5–100 μM). Inset: The calibration plot observed in the concentration range of 0–10 μM of DA.

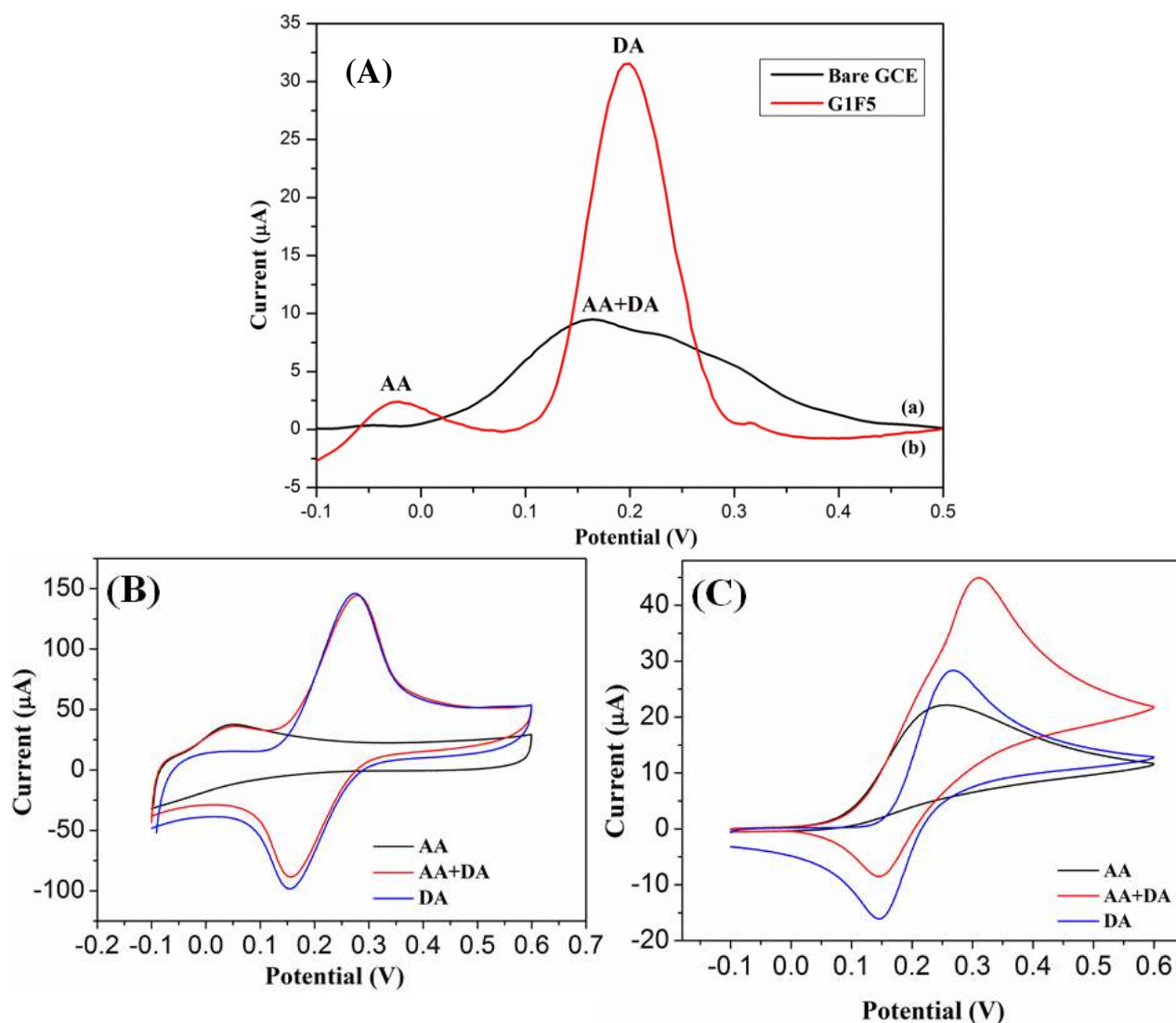


3.7. Selective Determination of DA in the Presence of AA

To evaluate the selectivity of electrochemical sensor, the influence of interfering species, ascorbic acid (AA) was examined in 0.1 M PBS containing 0.1 mM DA. Figure 9A shows the DPV responses of simultaneous oxidation of DA and AA at the bare GCE and G1F5/GCE electrodes. During the simultaneous detection of DA and AA at the bare GCE, the oxidation peak potentials of AA and DA are obviously overlapping and indefinable due to the poor selectivity. AA directly interferes with DA, so the bare GCE fails to determine the individual electrochemical redox peaks for DA (Figure 9A(a)). Interestingly, the G1F5/GCE modified electrode showed a significantly increased peak current for DA as well as the overlapped peak is resolved and clearly showed the individual electrocatalytic oxidation peaks for DA and AA at about 0.19 and 0.025 V, respectively (Figure 9A(b)). In addition, the strong electrostatic interaction and π - π conjugation emerged between the aromatic regions of positively charged DA and negatively charged G1F5 makes the electron transfer favorable and enhance the oxidation of DA to electrode surface, hence the AA oxidation is inactive and inhibited [37]. Figure 9A suggests that the G1F5/GCE has excellent electrocatalytic activity towards the oxidation of DA than

AA and exert no interference in the selective determination of DA. Further to confirm the selectivity of the G1F5/GCE, the cyclic voltammograms also recorded for DA, AA and DA+AA and are shown in Figure 9B and it can be clearly seen the DA and AA showed well resolved characteristic two peaks due to DA and AA. In contrast, peaks due to DA and AA are merged together in bare GCE (Figure 9C).

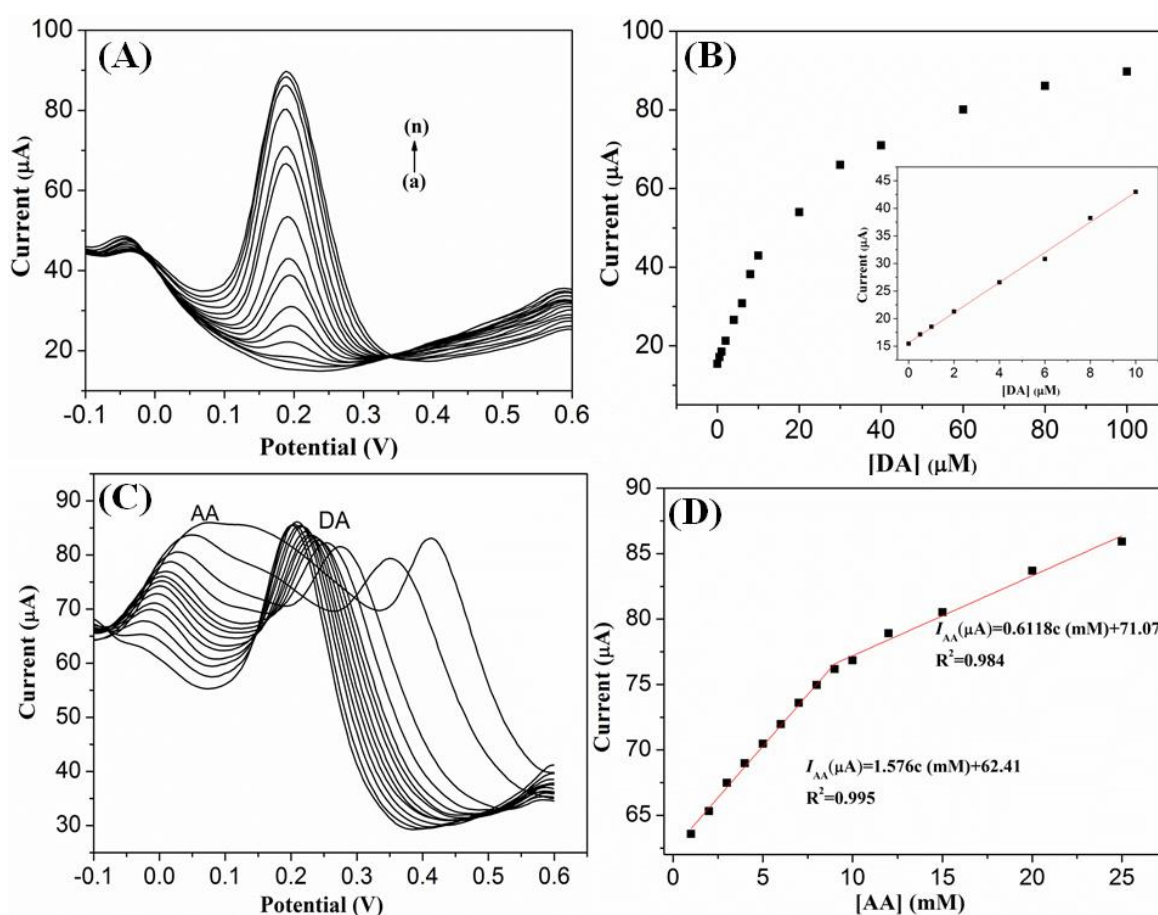
Figure 9. (A) DPV response observed for (a) bare GCE and (b) G1F5/GCE electrodes; CVs response obtained for (B) G1F5/GCE and (C) bare GCE in the presence of 0.1 mM of DA and 3 mM of AA in 0.1 M PBS (pH = 6.5).



The determination of DA is further investigated by differential pulse voltammetry (DPV) in the presence of AA. Figure 10A represents a series of DPV curves for the electrochemical oxidation currents for DA at a fixed concentration of 2 mM AA at G1F5/GCE. Figure 10A clearly represents that the DPV peak current for DA is linearly proportional with increasing concentration of DA in the solutions and two distinguish peaks correspond to the AA and DA are observed at about -46 and 189 mV, respectively. By varying the concentration of DA (0.5 – 100 μM), the anodic peak of AA is almost stable and no obvious changes in the peak current of AA are observed in the DPV curve.

Hence, the coexisting species AA has induced no interference effect in the determination of DA at the G1F5/GCE.

Figure 10. (A) DPV response of G1F5/GCE modified electrode with increasing the concentration of DA (from a to n: 0, 0.5, 1, 2, 4, 6, 8, 10, 20, 30, 40, 60, 80 and 100 μM) in the presence of 2 mM AA; (B) The relationship between the oxidation peaks current against DA concentrations (0.5–100 μM) in the presence of 2 mM AA. Inset: Enlarge view of calibration plot in the concentration range of 0–10 μM of DA; (C) DPVs response of G1F5/GCE modified electrode with various concentrations of AA (1–25 mM) in the presence of 0.1 mM DA; (D) Calibration plot obtained for oxidation peak current against AA concentrations.



The I_{pa} versus DA concentration curve in the range of 0–100 μM is displayed in Figure 10B. The linear regression equation was expressed as $I_{DA}(\mu\text{A}) = 15.64 + 2.733 C(\mu\text{M})$ with a correlation coefficient of 0.996 and a sensitivity of 2.733 $\mu\text{A}/\mu\text{M}$. The limit of detection (LOD) is estimated to be 0.12 μM ($S/N = 3$). Similarly, the electrochemical oxidation of AA was also investigated by varying the AA concentration while keeping the DA concentration as constant (0.1 mM) (Figure 10C). The peak current increased proportionally with increasing AA concentration. In addition, two different linear segments were observed in the calibration plots of peak currents versus AA concentration in the presence of 0.1 mM DA, corresponding to two different ranges of substrate concentration. The first linear segment ($I_{AA}(\mu\text{A}) = 62.41 + 1.576 C(\text{mM})$) corresponds to AA concentration from 1–9 mM, while the second linear segment ($I_{AA}(\mu\text{A}) = 71.07 + 0.6118 C(\text{mM})$) corresponds to AA concentration

from 9–25 mM (Figure 10D). The decrease in sensitivity (slope) at higher linear range of AA is attributed to the kinetic limitation of the G1F5 [38]. The detection limit for AA in the lower range and higher range are found out to be 0.42 μM and 2.77 μM , respectively. Furthermore, shift in the peak potential of AA is likely due to the acidic nature of AA that affects and changes the pH of the solution when excess AA was added [39,40]. Compared with other works (Table 2), it is noteworthy to mention that the modified electrode based on $\text{Fe}_3\text{O}_4/\text{rGO}$ nanocomposite greatly increases the electrocatalytic active sites and promotes the electron transfer in the detection of DA. Furthermore, the reproducibility of the G1F5/GCE was also evaluated by the repetitive electrochemical measurements in the solution containing 0.1 mM DA. The modified electrode gives a relative standard deviation (R.S.D) of around 3.0% after 10 successive measurements, implying good reproducibility of the modified electrode.

Table 2. Comparison of results for the determination of DA using different electrodes.

Electrode	Method	Interference	Linearity (μM)	Detection Limit (μM)	Ref.
CAT ^a /ZnONps/CPE ^b	CA, CPA	-	5–41	3	[41]
Nanostructured gold	DPV	AA	10–100	5	[42]
$\text{Cu}_2\text{O}/\text{GCE}$	CV	UA	0.1–10	0.01	[43]
TiO_2 -graphene/GCE	CV	UA, AA	5–200	2	[44]
2-Amino-thiazol (AT) film/GCE	DPV	UA	5–25	5	[45]
Graphene/GCE	CV	EP, UA, AA	2.5–100	0.5	[46]
CTAB ^c /GNSP ^d	DPV	AA	4–52	0.6	[47]
Meso- SiO_2/CPE	DPV	UA, AA	0.4–25	0.1	[48]
RGO-HDPPy ^e doped GCE	DPV	UA, AA	0.001–8	0.003	[49]
$\text{Fe}_3\text{O}_4/\text{rGO}/\text{GCE}$	DPV	AA	0.5–100	0.12	Present work

Footnotes: ^a Catalase; ^b Carbon Paste Electrode; ^c Cetyltrimethylammonium bromide; ^d Graphene nano-sheets; ^e Polypyrrole nanospheres with highly dispersibility.

4. Conclusions

In conclusion, $\text{Fe}_3\text{O}_4/\text{rGO}$ nanocomposites were successfully synthesized *via* a simple, cost-effective and green approach. A sensitive and selective electrochemical sensor with $\text{Fe}_3\text{O}_4/\text{rGO}$ nanocomposites was developed for the determination of DA in the presence of AA. The $\text{Fe}_3\text{O}_4/\text{rGO}$ nanocomposites modified electrode showed significantly improved peak current towards the oxidation of DA. The $\text{Fe}_3\text{O}_4/\text{rGO}$ based electrochemical sensor displayed excellent electrocatalytic activity and electron transfer rate towards the DA oxidation. Moreover, the sensor electrode showed good sensitivity, selectivity and low detection limit in the simultaneous detection of DA and AA. These results reveal that $\text{Fe}_3\text{O}_4/\text{rGO}/\text{GCE}$ could be a potential candidate for electrochemical and biosensor applications.

Acknowledgments

The authors are grateful to Ministry of Higher Education of Malaysia for sanctioning High Impact Research Grant (UM.C/625/1/HIR/MOHE/05) and University of Malaya for the Postgraduate Research Grant (PPP) (PG107-2012B) and UMRG programme grant (RP007C/13AFR).

Author Contributions

T.P-S and A.P wrote the main manuscript text and prepared all figures in text. A.P., H.N.M., L.H.N. and Y.S. reviewed the manuscript content.

Conflicts of Interest

The authors declare no conflict of interest regarding the publication of this article.

References

1. Obata, T. Dopamine efflux by mptp and hydroxyl radical generation. *J. Neural Transm.* **2002**, *109*, 1159–1180.
2. Mohammadi, M.; Akhondzadeh, S. Advances and considerations in attention-deficit/hyperactivity disorder pharmacotherapy. *Acta Med. Iran.* **2011**, *49*, 487–498.
3. Aurora, R.N.; Kristo, D.A.; Bista, S.R.; Rowley, J.A.; Zak, R.S.; Casey, K.R.; Lamm, C.I.; Tracy, S.L.; Rosenberg, R.S. The treatment of restless legs syndrome and periodic limb movement disorder in adults—an update for 2012: Practice parameters with an evidence based systematic review and meta-analyses. *Sleep* **2012**, *35*, 1039–1062.
4. Carrera, V.; Sabater, E.; Vilanova, E.; Sogorb, M.A. A simple and rapid hplc–ms method for the simultaneous determination of epinephrine, norepinephrine, dopamine and 5-hydroxytryptamine: Application to the secretion of bovine chromaffin cell cultures. *J. Chromatogr. B* **2007**, *847*, 88–94.
5. Xu, X.D.; Zhang, H.Y.; Shi, H.M.; Ma, C.L.; Cong, B.; Kang, W.J. Determination of three major catecholamines in human urine by capillary zone electrophoresis with chemiluminescence detection. *Anal. Biochem.* **2012**, *427*, 10–17.
6. Naccarato, A.; Gionfriddo, E.; Sindona, G.; Tagarelli, A. Development of a simple and rapid solid phase microextraction-gas chromatography–triple quadrupole mass spectrometry method for the analysis of dopamine, serotonin and norepinephrine in human urine. *Anal. Chim. Acta* **2013**, *810*, 17–24.
7. Liu, Y.; Huang, J.S.; Hou, H.Q.; You, T.Y. Simultaneous determination of dopamine, ascorbic acid and uric acid with electrospun carbon nanofibers modified electrode. *Electrochem. Commun.* **2008**, *10*, 1431–1434.
8. Mao, Y.; Bao, Y.; Gan, S.Y.; Li, F.H.; Niu, L. Electrochemical sensor for dopamine based on a novel graphene-molecular imprinted polymers composite recognition element. *Biosens. Bioelectron.* **2011**, *28*, 291–297.
9. Vashist, S.K.; Zheng, D.; Al-Rubeaan, K.; Luong, J.H.T.; Sheu, F.S. Advances in carbon nanotube based electrochemical sensors for bioanalytical applications. *Biotechnol. Adv.* **2011**, *29*, 169–188.
10. Tong, Y.; Li, Z.C.; Lu, X.F.; Yang, L.; Sun, W.N.; Nie, G.D.; Wang, Z.J.; Wang, C. Electrochemical determination of dopamine based on electrospun CeO₂/Au composite nanofibers. *Electrochim. Acta* **2013**, *95*, 12–17.

11. Singh, V.; Joung, D.; Zhai, L.; Das, S.; Khondaker, S.I.; Seal, S. Graphene based materials: Past, present and future. *Prog. Mater. Sci.* **2011**, *56*, 1178–1271.
12. Artiles, M.S.; Rout, C.S.; Fisher, T.S. Graphene-based hybrid materials and devices for biosensing. *Adv. Drug Deliv. Rev.* **2011**, *63*, 1352–1360.
13. Han, Q.; Wang, X.; Yang, Z.Y.; Zhu, W.Y.; Zhou, X.M.; Jiang, H.J. Fe₃O₄@rGO doped molecularly imprinted polymer membrane based on magnetic field directed self-assembly for the determination of amaranth. *Talanta* **2014**, *123*, 101–108.
14. Sun, Y.F.; Chen, W.K.; Li, W.J.; Jiang, T.J.; Liu, J.H.; Liu, Z.G. Selective detection toward Cd²⁺ using Fe₃O₄/rGO nanoparticle modified glassy carbon electrode. *J. Electroanal. Chem.* **2014**, *714–715*, 97–102.
15. Yin, H.S.; Zhou, Y.L.; Meng, X.M.; Tang, T.T.; Ai, S.Y.; Zhu, L.S. Electrochemical behaviour of Sudan I at Fe₃O₄ nanoparticles modified glassy carbon electrode and its determination in food samples. *Food Chem.* **2011**, *127*, 1348–1353.
16. Liu, Y.; Zhou, J.; Gong, J.; Wu, W.P.; Bao, N. The investigation of electrochemical properties for Fe₃O₄@Pt nanocomposites and an enhancement sensing for nitrite. *Electrochim. Acta* **2013**, *111*, 876–887.
17. Wu, D.; Li, Y.Y.; Zhang, Y.; Wang, P.P.; Wei, Q.; Du, B. Sensitive electrochemical sensor for simultaneous determination of dopamine, ascorbic acid, and uric acid enhanced by amino-group functionalized mesoporous Fe₃O₄@graphene sheets. *Electrochim. Acta* **2014**, *116*, 244–249.
18. Qian, J.; Yang, X.W.; Jiang, L.; Zhu, C.D.; Mao, H.P.; Wang, K. Facile preparation of Fe₃O₄ nanospheres/reduced graphene oxide nanocomposites with high peroxidase-like activity for sensitive and selective colorimetric detection of acetylcholine. *Sens. Actuators B* **2014**, *201*, 160–166.
19. Liu, M.L.; Chen, Q.; Lai, C.L.; Zhang, Y.Y.; Deng, J.H.; Li, H.T.; Yao, S.Z. A double signal amplification platform for ultrasensitive and simultaneous detection of ascorbic acid, dopamine, uric acid and acetaminophen based on a nanocomposite of ferrocene thiolate stabilized Fe₃O₄@Au nanoparticles with graphene sheet. *Biosens. Bioelectron.* **2013**, *48*, 75–81.
20. Lim, H.N.; Huang, N.M.; Lim, S.S.; Harrison, I.; Chia, C.H. Fabrication and characterization of graphene hydrogel via hydrothermal approach as a scaffold for preliminary study of cell growth. *Int. J. Nanomed.* **2011**, *6*, 1817–1823.
21. Su, J.; Cao, M.H.; Ren, L.; Hu, C.W. Fe₃O₄-graphene nanocomposites with improved lithium storage and magnetism properties. *J. Phys. Chem. C* **2011**, *115*, 14469–14477.
22. Lian, P.C.; Zhu, X.F.; Xiang, H.F.; Li, Z.; Yang, W.S.; Wang, H.H. Enhanced cycling performance of Fe₃O₄-graphene nanocomposite as an anode material for lithium-ion batteries. *Electrochim. Acta* **2010**, *56*, 834–840.
23. Pan, S.D.; Zhang, Y.; Shen, H.Y.; Hu, M.Q. An intensive study on the magnetic effect of mercapto-functionalized nano-magnetic Fe₃O₄ polymers and their adsorption mechanism for the removal of Hg(II) from aqueous solution. *Chem. Eng. J.* **2012**, *210*, 564–574.
24. Peng, L.; Qin, P.F.; Lei, M.; Zeng, Q.; Song, H.J.; Yang, J.; Shao, J.H.; Liao, B.H.; Gu, J.D. Modifying Fe₃O₄ nanoparticles with humic acid for removal of Rhodamine B in water. *J. Hazard. Mater.* **2012**, *209–210*, 193–198.

25. Radhakrishnan, S.; Krisnamoorthy, K.; Sekar, C.; Wilson, J.; Kim, S.J. A highly sensitive electrochemical sensor for nitrite detection based on Fe₂O₃ nanoparticles decorated reduced graphene oxide nanosheets. *Appl. Catal. B* **2014**, *148–149*, 22–28.
26. Fu, C.J.; Zhao, G.G.; Zhang, H.J.; Li, S. A facile route to controllable synthesis of Fe₃O₄/graphene composites and their application in lithium-ion batteries. *Int. J. Electrochem. Sci.* **2014**, *9*, 46–90.
27. Zhang, Y.X.; Cheng, Y.X.; Zhou, Y.Y.; Li, B.Y.; Gu, W.; Shi, X.H.; Xian, Y.Z. Electrochemical sensor for bisphenol a based on magnetic nanoparticles decorated reduced graphene oxide. *Talanta* **2013**, *107*, 211–218.
28. Angeles, G.A.; Lopez, B.P.; Pardave, M.P.; Silva, M.T.R.; Alegret, S.; Merkoci, A. Enhanced host-guest electrochemical recognition of dopamine using cyclodextrin in the presence of carbon nanotubes. *Carbon* **2008**, *46*, 898–906.
29. Huang, D.Q.; Chen, C.; Wu, Y.M.; Zhang, H.; Sheng, L.Q.; Xu, H.J.; Liu, Z.D. The determination of dopamine using glassy carbon electrode pretreated by a simple electrochemical method. *Int. J. Electrochem. Sci.* **2012**, *7*, 5510–5520.
30. Barnes, E.O.; O'Mahony, A.M.; Aldous, L.; Hardacre, C.; Compton, R.G. The electrochemical oxidation of catechol and dopamine on platinum in 1-ethyl-3-methylimidazolium bis(trifluoromethylsulfonyl)imide ([C₂mim][NTF₂]) and 1-butyl-3-methylimidazolium tetrafluoroborate ([C₄mim][BF₄]): Adsorption effects in ionic liquid voltammetry. *J. Electroanal. Chem.* **2010**, *646*, 11–17.
31. Laviron, E. General expression of the linear potential sweep voltammogram in the case of diffusionless electrochemical systems. *J. Electroanal. Chem. Interfacial Electrochem.* **1979**, *101*, 19–28.
32. Sun, W.; Wang, Y.H.; Zhang, Y.Y.; Ju, X.M.; Li, G.J.; Sun, Z.F. Poly(methylene blue) functionalized graphene modified carbon ionic liquid electrode for the electrochemical detection of dopamine. *Anal. Chim. Acta* **2012**, *751*, 59–65.
33. Sun, W.; Wang, X.; Wang, H.; Ju, X.; Xu, L.; Li, G.; Sun, Z. Application of graphene-SnO₂ nanocomposite modified electrode for the sensitive electrochemical detection of dopamine. *Electrochim. Acta* **2013**, *87*, 317–322.
34. Zhu, Z.H.; Qu, L.N.; Zeng, Y.; Sun, W.; Huang, X.T. Electrochemical detection of dopamine on a Ni/Al layered double hydroxide modified carbon ionic liquid electrode. *Sens. Actuators B* **2010**, *151*.
35. Qu, S.; Wang, J.; Kong, J.; Yang, P.Y.; Chen, G. Magnetic loading of carbon nanotube/nano-Fe₃O₄ composite for electrochemical sensing. *Talanta* **2007**, *71*, 1096–1102.
36. Brownson, D.A.C.; Munro, L.J.; Kampouris, D.K.; Banks, C.E. Electrochemistry of graphene: Not such a beneficial electrode material? *RSC Adv.* **2011**, *1*, 978–988.
37. Wu, L.; Feng, L.Y.; Ren, J.S.; Qu, X.G. Electrochemical detection of dopamine using porphyrin-functionalized graphene. *Biosens. Bioelectron.* **2012**, *34*, 57–62.
38. Ardakani, M.M.; Rajabi, H.; Beitollahi, H.; Mirjalili, B.B.F.; Akbari, A.; Taghavinia, N. Voltammetric determination of dopamine at the surface of TiO₂ nanoparticles modified carbon paste electrode. *Int. J. Electrochem. Sci.* **2010**, *5*, 147–157.

39. Gao, M.; Peh, C.K.N.; Ong, W.L.; Ho, G.W. Green chemistry synthesis of a nanocomposite graphene hydrogel with three-dimensional nano-mesopores for photocatalytic H₂ production. *RSC Adv.* **2013**, *3*, 13169.
40. Thien, S.H.; Pandikumar, A.; Huang, N.M.; Lim, H.N. Highly exposed {001} facets of titanium dioxide modified with reduced graphene oxide for dopamine sensing. *Sci. Rep.* **2014**, *4*, 5044.
41. Fooladsaz, K.; Negahdary, M.; Rahimi, G.; Tamijani, A.H.; Parsania, S.; Dastjerdi, H.A.; Sayad, A.; Jamaledin, A.; Salahi, F.; Asadi, A. Dopamine determination with a biosensor based on catalase and modified carbon paste electrode with zinc oxide nanoparticles. *Int. J. Electrochem. Sci.* **2012**, *7*, 9892–9908.
42. Plowman, B.J.; Mahajan, M.; O'Mullane, A.P.; Bhargava, S.K. Electrochemical detection of dopamine and cytochrome c at a nanostructured gold electrode. *Electrochim. Acta* **2010**, *55*, 8953–8959.
43. Zhang, F.Y.; Li, Y.J.; Gu, Y.; Wang, Z.H.; Wang, C.M. One-pot solvothermal synthesis of a Cu₂O/graphene nanocomposite and its application in an electrochemical sensor for dopamine. *Electrochim. Acta* **2011**, *173*, 103–109.
44. Fan, Y.; Lu, H.T.; Liu, J.H.; Yang, C.P.; Jing, Q.S.; Zhang, Y.X.; Yang, X.K.; Huang, K.J. Hydrothermal preparation and electrochemical sensing properties of TiO₂-graphene nanocomposite. *Colloids Surf. B* **2011**, *83*, 78–82.
45. Tsai, T.H.; Huang, Y.C.; Chen, S.M.; Ali, M.A.; AlHemaid, F.M.A. Fabrication of multifunctional biosensor for the determination of hydrogen peroxide, dopamine and uric acid. *Int. J. Electrochem. Sci.* **2011**, *6*, 6456–6468.
46. Ma, X.Y.; Chao, M.Y.; Wang, Z.X. Electrochemical detection of dopamine in the presence of epinephrine, uric acid and ascorbic acid using a graphene-modified electrode. *Anal. Methods* **2012**, *4*, 1687–1692.
47. Liu, S.Q.; Sun, W.H.; Hu, F.T. Graphene nano sheet-fabricated electrochemical sensor for the determination of dopamine in the presence of ascorbic acid using cetyltrimethylammonium bromide as the discriminating agent. *Sens. Actuators B* **2012**, *173*, 497–504.
48. Sun, D.; Xie, X.F.; Zhang, H.J. Surface effects of mesoporous silica modified electrode and application in electrochemical detection of dopamine. *Colloids Surf. B* **2010**, *75*, 88–92.
49. Qian, T.; Yu, C.F.; Wu, S.S.; Shen, J. In situ polymerization of highly dispersed polypyrrole on reduced graphite oxide for dopamine detection. *Biosens. Bioelectron.* **2013**, *50*, 157–160.